Atmospheric Chemistry of CHF_2CHO: Study of the IR and UV−Vis Absorption Cross Sections, Photolysis, and OH-, Cl-, and NO_3-Initiated Oxidation

Stig R. Sellevåg,[†] Yngve Stenstrøm,[‡] Trygve Helgaker,[†] and Claus J. Nielsen*[,†]

Department of Chemistry, University of Oslo, P.O. Box 1033 Blindern, N-0315 Oslo, Norway, and Department of Chemistry, Biotechnology and Food Science, Chemistry Section, Norwegian University of Life Sciences, P.O. Box 5003, N-1432 Aas, Norway

Received: January 18, 2005; In Final Form: March 1, 2005

The infrared and ultraviolet−visible absorption cross sections, effective quantum yield of photolysis, and OH, Cl, and NO_3 reaction rate coefficients of CHF_2CHO are reported. Relative rate measurements at 298 ± 2 K and 1013 ± 10 hPa gave $k_{OH} = (1.8 \pm 0.4) \times 10^{-12}$ cm^3 molecule^{-1} s^{-1} (propane as reference compound), $k_{Cl} = (1.24 \pm 0.13) \times 10^{-11}$ cm^3 molecule^{-1} s^{-1} (ethane as reference compound), and $k_{NO_3} = (5.9 \pm 1.7) \times 10^{-17}$ cm^3 molecule^{-1} s^{-1} (*trans*-dichloroethene as reference compound). The photolysis of CHF_2CHO has been investigated under pseudonatural tropospheric conditions in the European simulation chamber, Valencia, Spain (EUPHORE), and an effective quantum yield of photolysis equal to 0.30 ± 0.05 over the wavelength range 290−500 nm has been extracted. The tropospheric lifetime of CHF_2CHO is estimated to be around 1 day and is determined by photolysis. The observed photolysis rates of CH_3CHO, CHF_2CHO, and CF_3CHO are discussed on the basis of results from quantum chemical calculations.

1. Introduction

Recently, the atmospheric chemistry of CHF_2CH_2OH has been investigated.[1,2] It was found that 2,2-difluoroacetaldehyde, CHF_2CHO, is a primary degradation product in the gas-phase oxidation of the alcohol. CHF_2CHO is also a possible degradation product from the atmospheric oxidation of larger compounds containing a CHF_2CH_2 moiety. The interest in these compounds lies in the fact that partially fluorinated alcohols have been suggested as new hydrochlorofluorocarbon (HCFC) and hydrofluorocarbon (HFC) replacement compounds in certain industrial applications. To provide a balanced assessment of the environmental burden of these new HCFC/HFC replacement compounds, it is necessary to have information about the atmospheric fate of their oxidation products.

The major tropospheric sinks for CHF_2CHO in the gas phase will be reaction with OH radicals and photolysis. Reaction with Cl atoms can be of importance in marine boundary layers, while NO_3 radicals are important for the nighttime tropospheric chemistry. To quantify the atmospheric lifetime of CHF_2CHO, information about OH, Cl, and NO_3 reaction rate coefficients and photodissociation quantum yields are needed. This information for 2,2-difluoroacetaldehyde is deficient or nonexisting.

The atmospheric chemistry of 2,2-difluoroacetaldehyde has previously been investigated by Scollard et al,[3] who reported the following OH and Cl reaction rate coefficients of CHF_2CHO: $k_{OH}(298\pm2K) = (1.7 \pm 0.2) \times 10^{-12}$ cm^3 molecule^{-1} s^{-1} (laser photolysis−resonance fluorescence measurement) and $(1.4 \pm 0.3) \times 10^{-12}$ cm^3 molecule^{-1} s^{-1} (relative rate measurement); $k_{Cl}(298\pm2K) = (5.6 \pm 1) \times 10^{-12}$ cm^3 molecule^{-1} s^{-1} (relative rate measurement).

As part of our ongoing studies of the environmental impact of potential industrial HCFC and HFC replacement compounds[2,4,5] we have measured the IR and UV−vis absorption cross sections, the OH, Cl, and NO_3 reaction rate coefficients, and the tropospheric photolysis rate of 2,2-difluoroacetaldehyde. Quantum chemical calculations on the photolytic dissociation pathways of CHF_2CHO are also reported and compared to similar calculations on the photodissociation pathways of CH_3CHO, CH_2FCHO, and CF_3CHO.

2. Experimental and Computational Methods

2.1. Synthesis. 2,2-Difluoroacetaldehyde is not a commercially available compound. To our knowledge, two different ways of preparing CHF_2CHO have been reported in the literature: reduction of $CHF_2C(O)OH$[6] and preparation from a hemiacetal/hydrate mixture.[3,7]

1-Ethoxy-2,2-difluoroethanol was prepared by a slight modification of a literature procedure.[8] A solution of ethyl difluoroacetate (2.01 g; 16.2 mmol) in 10 mL of dry ether was cooled to −85 °C. Under vigorous stirring a solution of $LiAlH_4$ in ether (1.0 M; 6.0 mL; 6.0 mmol) was slowly added. The reaction was stirred for 4 h while heating to −75 °C. Ethanol (95%; 1.0 mL) was added and the mixture was allowed to heat up to room temperature and poured onto a mixture of crushed ice and concentrated H_2SO_4 (1.5 mL). Extraction with ether, drying ($MgSO_4$), and concentration by careful evaporation of the solvent left an oil, which by fractional distillation gave 1.45 g (71%) of 1-ethoxy-2,2-difluoroethanol: bp 59−61 °C (60 mmHg) [lit.[8] bp 45−47 °C (27 mmHg)]. All the spectroscopic data (FTIR and ^{1}H, ^{13}C, and ^{19}F NMR) were in accord with the literature.[8] 1-Ethoxy-2,2-difluoroethanol was stored in the dark at 277 K, and was stable over several weeks.

CHF_2CHO was synthesized by adding 1-ethoxy-2,2-difluoroethanol to concentrated sulfuric acid (95%). After ca. 15 min of mixing, CHF_2CHO was distilled off under vacuum and trapped in a container at liquid nitrogen temperature. The purity was estimated to be better than 95% (no traces of 1-ethoxy-

* Address correspondence to this author. Fax: +47 2285 5441. Phone: +47 2285 5680. E-mail: claus.nielsen@kjemi.uio.no.
[†] University of Oslo.
[‡] Norwegian University of Life Sciences.

10.1021/jp050313m CCC: $30.25
Published on Web 04/02/2005

2,2-difluoroethanol or ethanol could be observed in the infrared spectra). 2,2-Difluoroacetaldehyde rapidly undergoes polymerization and was therefore stored in the dark at 195 K.

2.2. Measurements of Absorption Cross Sections. From Beer−Lambert's law, the absorption cross section of a compound J at a specific wavenumber $\tilde{\nu}$ is given by $\sigma(\tilde{\nu}) = A_e/n_J l$, where $A_e = -\ln \tau(\tilde{\nu})$ is the napierian absorbance, τ is the transmittance, n_J is the number density of J, and l is the path length over which the absorption takes place. The integrated absorption intensity, S_{int}, is given by

$$S_{int} = \int_{band} \sigma(\tilde{\nu})\, d\tilde{\nu} \qquad (1)$$

Fourier transform infrared (FTIR) spectra of pure vapor of CHF_2CHO were recorded at 298 ± 2 K in the region 4000−400 cm^{-1}, using a Bruker IFS 113v spectrometer employing a nominal resolution of 1.0 cm^{-1} and Blackman-Harris 3-Term apodization of the interferograms. A Ge/KBr beam splitter was used to cover the spectral region, and a DTGS detector was chosen because of its linear response. Eight single channel spectra each recorded with 32 scans were averaged to yield one background or sample spectrum. Background spectra of an empty 2.34 ± 0.02 cm gas cell with KBr windows were recorded before and after each sample spectrum. In the case where the two background spectra were not similar, the background spectrum that gave the transmittance spectrum with best baseline in the nonabsorbing regions was used in the succeeding analysis. The partial pressures of the gases were in the range 2−10 hPa, and were measured by using an absolute pressure transducer (MKS Baratron Type 122A) with a stated accuracy of ±0.15%. Three independent experiments were performed.

Absorption cross sections in the UV−vis region were obtained at 298 ± 2 K with an Agilent 8453E photodiode array spectrophotometer. The spectra were recorded in the wavelength range from 190 to 1100 nm with sampling intervals of 1 nm, which gives a spectral resolution of 2 nm. The integration time was set to 0.5 s. The pressures of the pure vapors were in the range between 5 and 17 hPa, and were measured by using the Baratron pressure transducer mentioned above. A gas cell of 8.0 ± 0.1 cm length with quartz windows was used. The absorption cross sections were determined from three independent measurements.

2.3. Relative Rate Measurements. The OH, Cl, and NO_3 reaction rate coefficients of CHF_2CHO were determined by the relative rate method, in which the rate coefficient for the compound of interest is measured relative to a reference compound with a known rate coefficient. If the reactants react solely with the same radical and none of the reactants is reformed in any side reactions, the relative rate coefficient, k_{rel}, is given according to the following expression:

$$\ln\left\{\frac{[S]_0}{[S]_t}\right\} = k_{rel} \ln\left\{\frac{[R]_0}{[R]_t}\right\}, \qquad k_{rel} = \frac{k_S}{k_R} \qquad (2)$$

where S is the substrate and R is the reference compound. $[S]_0$, $[R]_0$, $[S]_t$, and $[R]_t$ are concentrations of S and R at the start and at the time t, respectively, and k_S and k_R are rate coefficients. The experiments were performed in purified air ($CO + NO_x$ < 100 ppb and C_nH_m < 1 ppm; delivered by AGA) at 298 ± 2 K and 1013 ± 10 hPa in a 250 L reaction chamber of electropolished stainless steel equipped with a multiple reflection White type mirror system adjusted to give a total optical path of 120 m. The optical system is connected to a Bruker IFS 66v FTIR spectrometer with MCT detector, allowing in situ monitoring. In all experiments, FTIR spectra were recorded in the wavenumber range 4500−400 cm^{-1}. Each spectrum was recorded by co-adding 100 scans and employing a nominal resolution of 0.5 cm^{-1} and Happ-Genzel apodization (collection time ca. 2 min). Initial mixing ratios of the reactants in the reaction chamber were 1−4 ppm. The following reference compounds were used: propane (99.95%; AGA) in the OH experiments, ethane (99.0%; AGA) in the Cl experiments, and (*E*)-$C_2H_2Cl_2$ (98%; Aldrich) in the NO_3 experiments.

OH radicals were generated by photolysis of O_3 in the presence of H_2 (99%; AGA). Ozone was produced by discharge of oxygen (99.95%; AGA), where approximately 2% of the oxygen gas was converted to ozone. Typical mixing ratios of ozone and hydrogen were 3×10^2 and 5×10^3 ppm, respectively. Photolysis of ozone was carried out in intervals of 1−2 min, using two Philips TL 20W/12 fluorescence lamps (λ_{max} ∼310 nm). This OH production method produces OH radicals not only in the ground state but also in excited vibrational states.[9−11] The collision quenching rate coefficients of OH by N_2 and O_2 is of the order of 10^{-15} and 10^{-13} cm^3 $molecule^{-1}$ s^{-1}, respectively.[12] However, the mixing ratios of O_2 and N_2 are 5 orders of magnitude larger than that of the CHF_2CHO, and one may therefore safely assume that this compound reacts exclusively with OH in the vibrational ground state.

Chlorine atoms were generated by photolysis of 20−25 ppm chlorine gas (99.8%; AGA) employing two Philips TLD 18W/08 fluorescence lamps (λ_{max} ∼375 nm). In this wavelength region the Cl atoms produced were in the ground state. The photolysis was carried out at intervals of 15−60 s.

NO_3 radicals were generated by thermal decomposition of N_2O_5 (∼50 ppm). N_2O_5 was synthesized by mixing gas streams of O_3 and NO_2 (99.0%; AGA), trapping the products at 195 K. N_2O_5 was purified by vacuum distillation prior to its use.

All reactants were stable in the dark in the reaction chamber. However, CHF_2CHO was not photolytically stable during irradiation by the Philips TL 20W/12 fluorescence lamps (λ_{max} ∼310 nm). The photolysis rate coefficient of CHF_2CHO under these conditions was therefore determined from three separate experiments.

2.4. EUPHORE Experiments. The photolysis of CHF_2CHO was studied under pseudonatural conditions in the EUPHORE simulation chamber in Valencia, Spain (longitude = −0.5°, latitude = 39.5°). The date of the experiment was October 21, 2004 (initial dew point: −36.2 °C). Technical information concerning the installation has been previously reported in the literature.[13−17] For brevity, only brief details will therefore be given here. The experiments were performed in chamber B in purified air (see Becker[13] for a description of the drying and purification system). This chamber was equipped with a Nicolet Magna 550 FTIR spectrometer coupled with a White multireflection mirror system for in situ analysis adjusted to give an optical path length of 553.5 m. FTIR spectra were recorded every 5 min by co-adding 270 interferograms with a resolution of 1.0 cm^{-1}. Additional analyses were carried out with a gas chromatograph (Fisons Instruments GC 8000 Series) equipped with a photoionization detector.

Loss of the aldehyde in the chamber is due to photolysis, reaction with OH radicals, and leakage. The leakage rate was measured by adding ca. 29 ppb of SF_6 to the reaction chamber. The loss due to OH reactions was quantified by adding 47 ppb of di-*n*-butyl ether (DNBE, $(C_4H_9)_2O$) (99.3%; Aldrich) to the reaction chamber since the disappearance of DNBE is solely

TABLE 1: Reaction Scheme Used for Determining the Observed Photolysis Rate, J_{obs}, of CHF_2CHO

reaction	rate coefficient
$CHF_2CHO + h\nu \rightarrow$ products	J_{obs}
$CHF_2CHO + OH \rightarrow$ products	k_{ald} [a]
$CHF_2CHO \rightarrow$ loss by leakage	$k_{leak}(t)$ [b]
$(C_4H_9)_2O + OH \rightarrow$ products	k_{DNBE} [c]
$(C_4H_9)_2O \rightarrow$ loss by leakage	$k_{leak}(t)$ [b]
$SF_6 \rightarrow$ loss by leakage	$k_{leak}(t)$ [b]

[a] $k_{ald} = 1.8 \times 10^{-12}$ cm^3 molecule^{-1} s^{-1} (this work). [b] See eq 5 and text for details. [c] $k_{DNBE} = 2.89 \times 10^{-11}$ cm^3 molecule^{-1} s^{-1}.[46]

due to its reaction with OH radicals and leakage. The observed losses of SF_6, DNBE, and CHF_2CHO were subsequently corrected for variations in pressure and temperature with use of the ideal gas law. The loss processes in the chamber and their rate coefficients are summarized in Table 1.

The effective quantum yield of photolysis is given as the ratio

$$\Phi_{eff} = J_{obs}/J_{max} \quad (3)$$

where J_{obs} is the observed photolysis rate coefficient and J_{max} is the maximum photolysis rate coefficient given by

$$J_{max} = \int \sigma(\lambda)\phi(\lambda)F(\lambda)\, d\lambda \quad (4)$$

Here $\sigma(\lambda)$ is the absorption cross section (base e) of the aldehyde (in units of cm^2 molecule^{-1}), $\phi(\lambda)$ is the quantum yield ($\phi(\lambda) = 1$), and $F(\lambda)$ is the solar actinic flux (photons cm^{-2} s^{-1}) measured with a spectral radiantmeter. The specifications of the radiantmeter are given by Wenger et al.[17] The integration was carried out over the wavelength range 290−500 nm.

2.5. Electronic Structure Calculations. MP2,[18] B3LYP,[19,20] and CCSD(T)[21] calculations were carried out with the Gaussian 98 program.[22] Unrestricted wave functions were used to describe open shell systems and bond breaking processes; singlet ground-state structures were calculated by using a restricted wave function. The core electrons were kept frozen in the MP2 and CCSD(T) calculations. Dunning's correlation-consistent aug-cc-pV*X*Z (X = D, T, Q) basis sets[23,24] were employed in all calculations. The Franck−Condon region of the potential energy surfaces was explored by calculating vertical excitation energies, using time-dependent density functional theory (TDDFT)[25,26] and the B3LYP functional.

Complete active space calculations (CAS)[27,28] were carried out with use of the Dalton program.[29] As a starting point for the CAS calculations, the ground-state potential energy surface of CH_3CHO was probed at the HF/aug-cc-pVDZ level of theory. The strategy was to construct an active space capable of describing the bond dissociations and the $\pi^* \leftarrow$ n transition of the carbonyl group. The smallest active space must therefore consist of the bonding and antibonding carbon−carbon and carbon−carbonyl hydrogen σ orbitals, the bonding and antibonding π orbitals, and the highest occupied lone-pair orbital (n) on oxygen, i.e., 8 electrons in 7 orbitals, denoted by CAS-(8,7). The orbitals were moved into the active space by stretching the relevant bonds, using the MP2 natural orbitals start orbitals for the CAS calculations.[30] Effects due to the size of the active space were tested by increasing the active space to 12 electrons in 12 orbitals.

3. Results and Discussion

3.1. IR and UV−Vis Absorption Cross Sections. The infrared absorption cross sections (base e) were obtained from the absorbance spectra assuming that the gas was ideal and applying a baseline correction. The baseline correction was performed by subtracting a polynomial function, obtained by fitting the regions of the spectrum where no absorptions were expected. The integrations over the absorption bands were carried out by using a method that defines the baseline from an average of two points on one side of the band and the average of two points on the other side of the band.

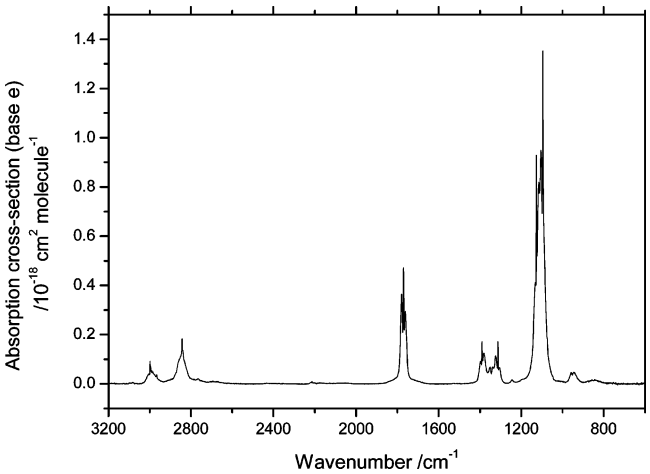

Figure 1. Infrared absorption cross sections (base e) of pure vapor of CHF_2CHO at 298 ± 2 K.

TABLE 2: Absolute Absorption Intensities, S_{Int}, of Pure CHF_2CHO Vapor at 298 ± 2 K

wavenumber range/cm^{-1}	S_{int}/10^{-17} cm molecule^{-1}
1550−760	5.86 ± 0.07
1920−1630	1.270 ± 0.018
3115−2550	1.14 ± 0.04

The integrated absorption intensities of the absorption bands, or regions of overlapping bands, were determined by plotting the integrated absorbance against the product of the number density and the path length. As none of the regression lines had a *y*-intercept significantly different from zero, a least-squares method that forced the regression line to go through zero was used to determine the absorption intensities.

Figure 1 shows the absorption cross sections of CHF_2CHO in the 3200−600 cm^{-1} region (also given as Supporting Information in JCAMP-DX format). The integrated absorption intensities given in Table 2 have uncertainties less than 5%, and include, in addition to random errors, also errors in pressure measurements (0.15%), path length (0.90%), and temperature (0.67%). To assess the quality of the cross section data, our experimental setup has been tested against the well-studied HCFC-22 ($CHClF_2$).[31] The integrated absorption intensities obtained were within 5% of the average values reported in the intercomparison by Ballard et al.[31] We therefore believe that our measurements of CHF_2CHO are not affected by any large, unknown systematic errors other than those already quantified.

Figure 2 shows the UV−vis absorption cross sections of CHF_2CHO. The absorption band corresponds to the weak $\pi^* \leftarrow$ n transition of the carbonyl group. At the wavelength of maximum absorption (309 nm), the uncertainty in the absorption cross section is 0.3% (2σ). When errors in pressure measurements, path length, and temperature are taken into consideration, it is estimated that the absolute error limits are at most ±5%. The UV−vis absorption cross sections of CHF_2CHO are given as Supporting Information in JCAMP-DX format.

The UV−vis absorption cross sections of CHF_2CHO are only slightly lower than those of CH_3CHO.[32] However, the UV

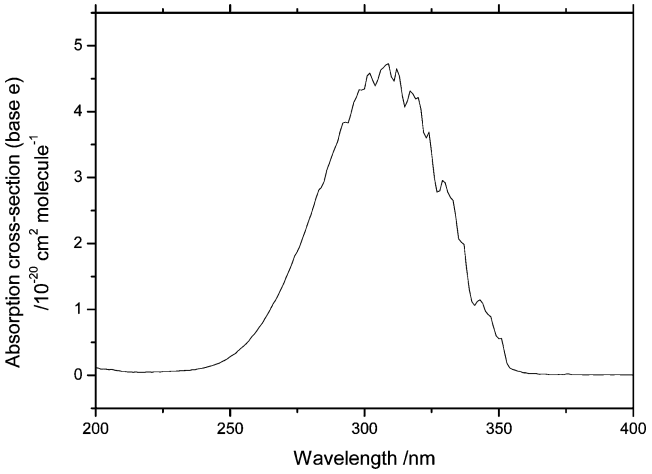

Figure 2. Ultraviolet−visible absorption cross sections (base e) of pure CHF_2CHO vapor at 298 ± 2 K.

spectrum of CHF_2CHO is red-shifted by ca. 19 nm. Interestingly, the UV spectrum of CHF_2CHO is also red-shifted by ca. 9 nm compared to that of CF_3CHO.[33−37]

3.2. OH, Cl, and NO_3 Reaction Rate Coefficients. Losses of reactant and reference compounds were monitored by online FTIR detection. A spectral subtraction procedure was used to determine the relative concentrations of the substrate and the reference compound at different time intervals. Based on the residuals from the spectral subtraction analysis, the uncertainty in the relative concentrations of the reactants was estimated to be 1%. The relative rate coefficients were determined according to eq 2 by using a weighted least-squares method that includes uncertainties in the concentrations of both reactants obtained by the spectral subtraction procedure.[38] The reported uncertainties in this work represent 2σ from the statistical analyses of the kinetic data and include uncertainties in the reaction rate coefficients of the reference compounds.

As mentioned previously, CHF_2CHO was not photostable during irradiation by the Philips TL 20W/12 fluorescence lamps having λ_{max} ~310 nm. A difference spectrum after 45 min of photolysis (only CHF_2CHO in the reaction chamber) is shown in Figure S1 (Supporting Information). There is clearly a formation of CO and CF_2O as photolysis products. No other products could be detected, which implies that the reaction route yielding CH_2F_2 is of minor importance (see later). The photolysis rate coefficient of CHF_2CHO was determined from three independent experiments, and a plot of $\ln\{[CHF_2CHO]_0/[CHF_2CHO]_t\}$ vs photolysis time is shown in Figure S2 (Supporting Information). The *y*-intercept of the plot was not significantly different from zero. A least-squares method that forced the regression line to go through zero was therefore used, and a photolysis rate coefficient of $k_{photol} = (2.01_1 \pm 0.05_7) \times 10^{-5}$ s^{-1} was extracted. However, OH radicals will eventually be produced as a result of photolysis ($CHF_2CHO + h\nu \rightarrow CHF_2 + HCO$ or $CHF_2CO + H$) and therefore in principle contribute to the observed loss of 2,2-difluoroacetaldehyde. We have modeled the photolytic and OH-initiated oxidation of 2,2-difluoroacetaldehyde in the reaction chamber using a general FACSIMILE[39] model, which includes 220 equations describing O_x, HO_x, NO_x, FO_x, ClO_x, BrO_x, and organic "background" reactions in the chamber (eight of them are photolysis reactions). The model showed that the degradation of 2,2-difluoroacetaldehyde by OH radicals is negligible in the present photolysis experiments.

The OH reaction rate coefficient of CHF_2CHO was determined relative to that of C_3H_8. The spectral subtraction analysis

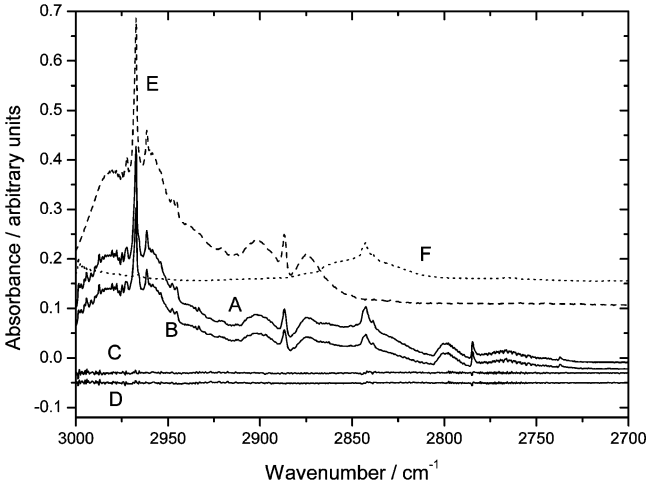

Figure 3. FTIR spectra of the reaction mixture $CHF_2CHO/C_3H_8/H_2/O_3$: (A) before reaction with OH; (B) after reaction with OH; (C) residual after spectral subtraction analysis of spectrum A, see text for a list of reference spectra included in the subtraction; (D) residual after spectral subtraction analysis of spectrum B; (E) reference spectrum of CHF_2CHO; and (F) reference spectrum of C_3H_8. The spectra C−F have been shifted for clarity.

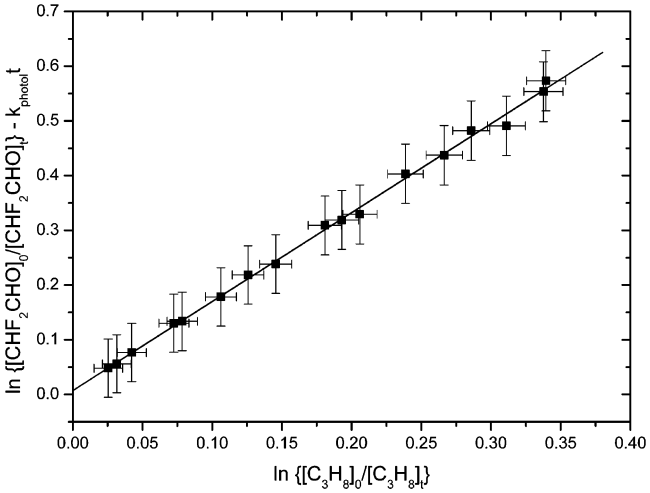

Figure 4. Decay of CHF_2CHO versus C_3H_8 in the presence of OH radicals at 298 ± 2 K as measured from three independent experiments (17 data points). The uncertainty in each data point is based on an estimated uncertainty of 0.01 in the relative concentrations. The decay of CH_2FCHO in the reaction chamber has been corrected for loss due to photolysis, see text for details. Least-squares analysis gave a relative rate coefficient of $1.62_6 \pm 0.04_2$ (*y*-intercept: 0.007 ± 0.008). The uncertainty of the linear regression coefficients represents 2σ.

was carried out over the wavenumber region 3000−2700 cm^{-1}, i.e., part of the C−H stretching region, to determine the relative concentrations of both 2,2-difluoroacetaldehyde and propane. FTIR reference spectra of C_3H_8, CHF_2CHO, CH_3COCH_3, O_3, HCHO, and H_2O and a sloping baseline were included in the spectral subtraction analyses. An example of the residuals after the spectral subtraction is shown in Figure 3.

Figure 4 shows a plot of the decay of 2,2-difluoroacetaldehyde vs the decay of propane due to reaction with OH radicals in three independent experiments. The loss of 2,2-difluoroacetaldehyde has been corrected for loss due to photolysis. A least-squares analysis of the data gave a relative OH reaction rate coefficient of $1.62_6 \pm 0.04_2$ (2σ). The latest JPL data evaluation[40] and the IUPAC Subcommittee on Gas Kinetic Data Evaluation for Atmospheric Chemistry[41] has recommended a rate coefficient of $k(OH+C_3H_8) = 1.1 \times 10^{-12}$ cm^3 $molecule^{-1}$

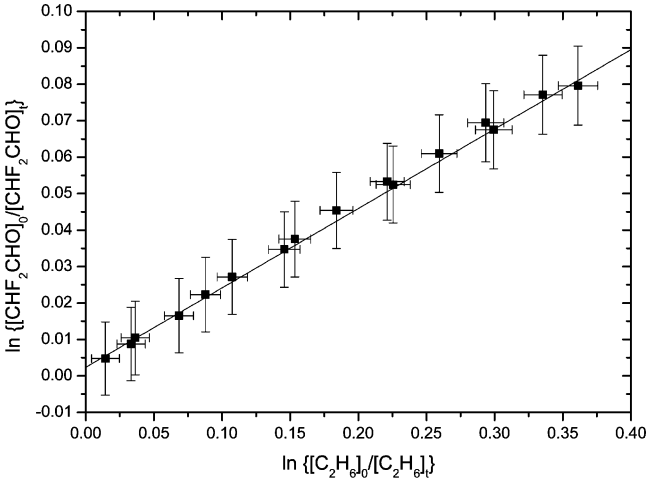

Figure 5. Decay of CHF_2CHO versus C_2H_6 in the presence of Cl atoms at 298 ± 2 K as measured from two independent experiments (16 data points). The uncertainty in each data point is based on an estimated uncertainty of 0.01 in the relative concentrations. Least-squares analysis gave a relative rate coefficient of 0.218 ± 0.006 (*y*-intercept: 0.002 ± 0.0012). The uncertainty of the linear regression coefficients represents 2σ.

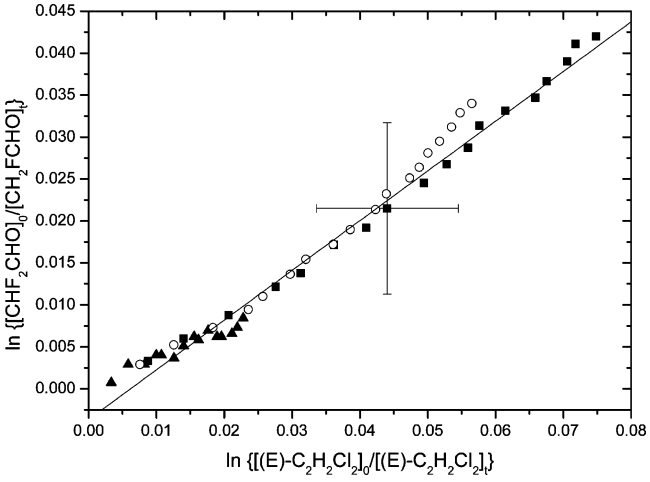

Figure 6. Decay of CHF_2CHO versus (*E*)-$C_2H_2Cl_2$ in the presence of NO_3 radicals at 298 ± 2 K as measured from three independent experiments (51 data points). The uncertainty in each data point is based on an estimated uncertainty of 0.01 in the relative concentrations (only one error bar is shown). Least-squares analysis gave a relative rate coefficient of 0.592 ± 0.028 (*y*-intercept: −0.0037 ± 0.0014). The uncertainty of the linear regression coefficients represents 2σ. See text for a discussion of the curvature of the plot.

s^{-1} at 298 K with an uncertainty factor of 1.2. On an absolute scale the OH reaction rate coefficient of 2,2-difluoroacetaldehyde is then $(1.8 \pm 0.4) \times 10^{-12}$ cm^3 $molecule^{-1}$ s^{-1} (uncertainty in the absolute rate coefficient of propane included).

Scollard et al.[3] reported two values for the OH reaction rate coefficient of CHF_2CHO: one measured by laser photolysis−resonance fluorescence (LP-RF), $(1.7 \pm 0.2) \times 10^{-12}$ cm^3 $molecule^{-1}$ s^{-1}, and one measured by the relative rate method, $(1.4 \pm 0.3) \times 10^{-12}$ cm^3 $molecule^{-1}$ s^{-1}, using toluene ($C_6H_5CH_3$) as the reference compound. There is very good agreement between the rate coefficient from the present work and the one determined by the LP-RF technique by Scollard and co-workers. However, our rate coefficient is almost 30% larger, but not significantly different, than the rate coefficient measured by the relative rate technique in the paper by Scollard et al.[3] Scollard and co-workers used 5.96×10^{-12} cm^3 $molecule^{-1}$ s^{-1} (from the evaluations by Atkinson[42,43]) as the rate coefficient for the reaction between OH and toluene. More recent measurements[44−47] are all in agreement with the evaluations by Atkinson,[42,43] suggesting that it is a reasonable value to use. Still there is about 20−25% uncertainty associated with the rate coefficients of the reference compounds, making up for most of the discrepancy between the relative rate measurements presented in this work and in the paper by Scollard et al.[3] We also note that there is ca. 20% uncertainty in the relative rate coefficient measured by Scollard and co-workers, which refers to precision only.

Ethane, C_2H_6, was used as the reference compound to determine the Cl reaction rate coefficient of 2,2-difluoroacetaldehyde. The relative concentrations of the two compounds were extracted by analyzing the spectral region 2950−2600 cm^{-1}. FTIR reference spectra of CHF_2CHO, C_2H_6, CH_3CHO, HCHO, and HCl and a sloping baseline were included in the spectral subtraction. An example of the residuals after the subtraction is shown in Figure S3 (Supporting Information).

A least-squares analysis of the $\ln\{[CHF_2CHO]_0/[CHF_2CHO]_t\}$ vs $\ln\{[C_2H_6]_0/[C_2H_6]_t\}$ data, shown in Figure 5, gave a relative rate coefficient of 0.218 ± 0.006 (2σ). The recommended Cl reaction rate coefficient of ethane is 5.7×10^{-11} cm^3 $molecule^{-1}$ s^{-1} with an uncertainty factor of 1.1.[40] This gives an absolute rate coefficient of $(1.24 \pm 0.13) \times 10^{-11}$ cm^3 $molecule^{-1}$ s^{-1} for the reaction between CHF_2CHO and Cl atoms. This value is a factor of 2 larger than that reported by Scollard et al.,[3] $(5.6 \pm 1.0) \times 10^{-12}$ cm^3 $molecule^{-1}$ s^{-1}, who also used the relative rate method for determining the rate coefficient, but with acetone as reference compound and $k(Cl+CH_3C(O)CH_3) = 2.37 \times 10^{-12}$ cm^3 $molecule^{-1}$ s^{-1}.[48] The latest JPL evaluation has recommended 2.7×10^{-12} cm^3 $molecule^{-1}$ s^{-1} as the Cl rate coefficient of acetone with an uncertainty factor of 1.3. Using this value places the Cl rate coefficient of 2,2-difluoroacetaldehyde of Scollard and co-workers at $(6.4 \pm 2.2) \times 10^{-12}$ cm^3 $molecule^{-1}$ s^{-1}, still significantly different from our measurement. Obviously the two results cannot both be correct. We cannot comment on the kinetic result by Scollard and co-workers as their data for this reaction are not presented. We note that their relative rate coefficient has an uncertainty of 18%, which refers to precision only. We also note, although this does not prove anything, that our values for k_{OH} and k_{Cl} of CHF_2CHO will fit the correlation line of the linear free energy plot for halogenated aldehydes (Figure 5 in ref 3).

The NO_3 reaction rate coefficient of 2,2-difluoroacetaldehyde was measured relative to that of *trans*-dichloroethene ((*E*)-$C_2H_2Cl_2$). Atkinson et al.[49] and Noremsaune et al.[50] have measured the NO_3 rate coefficient of (*E*)-$C_2H_2Cl_2$, both reporting $k = (1.0 \pm 0.2) \times 10^{-16}$ cm^3 $molecule^{-1}$ s^{-1}. The spectral region 3200−2700 cm^{-1} was analyzed to extract the relative concentrations of the substrate and the reference compound. Reference spectra of 2,2-difluoroacetaldehyde, *trans*-dichloroethene, N_2O_5, HNO_3, and NO_2 together with a sloping baseline were included in the spectral subtraction analyses, see Figure S4 (Supporting Information) for FTIR spectra of the reaction mixture and the residual after spectral subtraction from one of the experiments.

A plot of $\ln\{[CHF_2CHO]_0/[CHF_2CHO]_t\}$ vs $\ln\{[(E)\text{-}C_2H_2Cl_2]_0/\{[(E)\text{-}C_2H_2Cl_2]_t\}$ from three independent experiments is given in Figure 6. The data points from each of the experiments are shown with different symbols; a single *x*,*y*-error bar indicating a representative uncertainty in the data points is also given. The rate of this reaction is on the limit of what we can determine in our chamber and the data points deviate considerably from the ideal straight line. This deviation, however, reflects the uncertainty of our spectral subtraction procedure rather than interfering secondary reactions (corroborated by our FAC-

SIMILE model of the reaction system). The spectral subtraction is also complicated due to the many overlapping absorption bands in the spectral region analyzed.

A least-squares analysis of the data points shown in Figure 6 gave a relative rate coefficient of 0.592 ± 0.028 (2σ). Considering the estimated uncertainties in this experiment, represented by the error bars in Figure 6, we prefer to quote a relative error of 20% in the relative rate coefficient instead of the 5% (2σ) from the statistical analysis, that is $k_{rel} = 0.59 \pm 0.12$. We therefore report $(5.9 \pm 1.7) \times 10^{-17}$ cm^3 molecule^{-1} s^{-1} as the rate coefficient for the reaction between CHF_2CHO and NO_3 (uncertainty in the rate coefficient of the reference compound has been included).

Despite its rather large uncertainty, this is a very interesting result. D'Anna et al.[51] have performed a kinetic study of OH and NO_3 radical reactions with 14 aliphatic aldehydes and correlated the NO_3 and OH rate coefficients according to a linear free energy relationship. They reported that the rate coefficients of the 14 aliphatic aldehydes all fell on a correlation line for addition reactions given by $\log k(NO_3) = (3.43 \pm 0.24) \times \log k(OH) + (22.7 \pm 2.5)$ and not on the correlation line for H-abstraction reactions given by $\log k(NO_3) = (0.87 \pm 0.09) \times \log k(OH) + (-6.0 \pm 1.0)$. This was attributed to inductive effects of the alkyl chain on the stability of the transition state and to formation of prereaction adducts.[51,52] For 2,2-difluoroacetaldehyde the predicted NO_3 rate coefficient using the correlation line for addition reactions is 2×10^{-18} cm^3 molecule^{-1} s^{-1}, more than 10 times lower than what was measured, while using the correlation line for H-abstraction reactions gives 6×10^{-17} cm^3 molecule^{-1} s^{-1}, which is in agreement with the observation. One should be careful drawing general conclusions based on one measurement, but it seems obvious that the conclusions about the reactivity of aliphatic aldehydes toward NO_3 radicals cannot be transferred directly to the reactivity of fluorinated aldehydes. In the following we will try to point in a direction where an explanation may be sought.

To gain more insight into the chemical reactivity of 2,2-difluoroacetaldehyde, we have performed quantum chemical calculations on the OH reaction of CHF_2CHO at the CCSD(T)/aug-cc-pVDZ//MP2/aug-cc-pVDZ level of theory. Optimally, it would have been best to perform these calculations on the $CHF_2CHO + NO_3$ reaction system. However, it is very difficult to perform quantum chemical calculations on this reaction system on a reasonable reliable level for two reasons: First, the electronic ground state of the nitrate radical is degenerate, which is difficult in itself to handle because of the "symmetry dilemma".[53] A multi-configurational wave function should therefore be used to describe the nitrate radical reliably.[54] Second, the size of the system makes the calculations very resource demanding. Consequently, we have restricted our calculations to the $CHF_2CHO + OH$ reaction system.

We have chosen CCSD(T)/aug-cc-pVDZ//MP2/aug-cc-pVDZ as our computational method because it offers direct comparison with the results of D'Anna et al.[52] on the OH reaction of acetaldehyde. We have investigated the barriers toward three different routes for the OH reaction of CHF_2CHO: (i) abstraction of the aldehydic hydrogen, (ii) abstraction of the α-hydrogen, and (iii) addition of OH to the carbonyl carbon. For brevity, we do not include structures of the optimized stationary points here, but refer to Figure S5a−h (Supporting Information) where they are displayed.

Figure 7 shows the calculated energy level diagram for the three different reaction routes. As can be seen, the abstraction

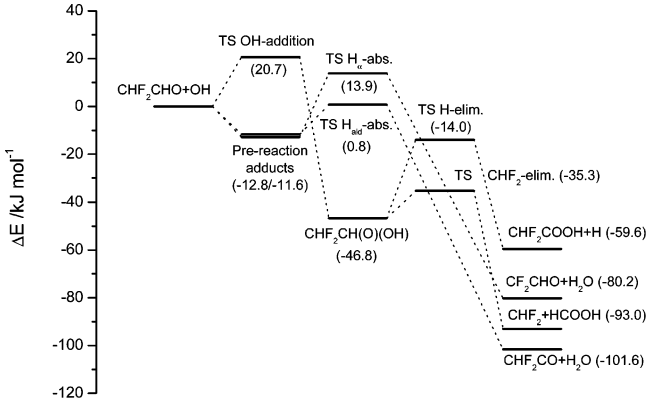

Figure 7. Energy level diagram for the reaction between CHF_2CHO and OH calculated at the CCSD(T)/aug-cc-pVDZ//MP2(FC)/aug-cc-pVDZ level of theory. Three different reaction routes have been investigated: (i) abstraction of the carbonyl hydrogen, (ii) abstraction of the α-hydrogen, and (iii) addition of OH to the carbonyl carbon. Structures of the stationary points are given in Figure S5. Zero-point vibrational energies are included in the energy differences.

of the aldehydic hydrogen proceeds with a small barrier of 0.8 kJ mol^{-1} while the barrier toward abstraction of the α-hydrogen is almost 14 kJ mol^{-1}. The addition reaction is not an important route as the barrier height is more than 20 kJ mol^{-1}. Similar to the $CH_3CHO + OH$ reaction system,[52,55,56] OH also forms prereaction adducts with CHF_2CHO, but they are ∼8 kJ mol^{-1} less stable than what was found for the $CH_3CHO + OH$ reaction system at the same computational level.[52] In contrast to what was found for the $CH_3CHO + OH$ reaction system, it has not been possible to locate any postreaction adducts involving water and the CHF_2CO radical. Weaker adducts can be explained by the fact that the fluorine atoms on the methyl group of CHF_2CHO will withdraw electron density from the oxygen atom making the hydrogen bond between OH and the aldehyde weaker. This picture is consistent with the results presented by Mora-Diez et al.[57] on the OH reactions with FCHO and ClCHO.

Smith and Ravishankara[58] have contended that adduct formation increases the rate coefficient for the OH reaction relative to that for the Cl atom and points to the OH and Cl reactions of HNO_3 and CH_3ONO_2 as examples. The OH reaction of nitric acid is strongly influenced by the presence of a prereaction adduct, while the OH reaction of CH_3ONO_2 is not, even though the two reaction systems are very similar. For CH_3ONO_2 the Cl reaction rate coefficient is an order of magnitude larger than the OH rate coefficient at room temperature. For 2,2-difluoroacetaldehyde, the ratio k_{Cl}/k_{OH} is ∼7, while it is ∼5 for acetaldehyde.[41] One might therefore expect the OH reaction of 2,2-difluoroacetaldehyde to be less affected by the presence of the prereaction adduct than in the case of acetaldehyde. It is reasonable to expect that this is also the case for the NO_3 reaction and thereby explains why the pair of OH/NO_3 rate coefficients of 2,2-difluoroacetaldehyde fall on the correlation line for abstraction reactions and not on the line for addition reactions. We stress, however, that we have not provided any strict evidence for this.

3.3. Photolysis. The photolysis of CHF_2CHO was studied under pseudonatural tropospheric conditions in the EUPHORE reaction chamber in Valencia, Spain. The initial mixing ratio of CHF_2CHO in the chamber was ∼70 ppb.

The decay of SF_6 with time in the reaction chamber is indicated in Figure 8. Normally such logarithmic plots are linear as the leakage of SF_6 from the chamber is a first-order process with a constant loss rate. The obvious curvature suggests that the leakage rate coefficient changed with the time of day. The

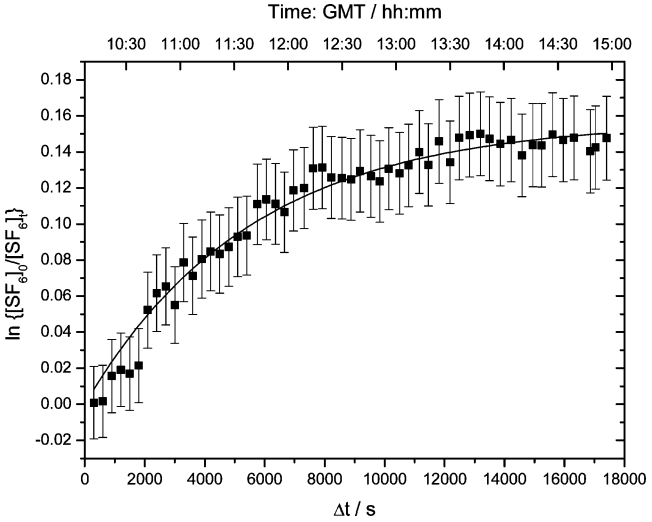

Figure 8. Leakage as measured from the disappearance of SF6 during the photolysis experiment with CHF_2CHO in the EUPHORE simulation chamber. The data points have been corrected for variations in pressure and temperature during the experiment. The observed leakage has been fitted according to eq 5, where $a = 0.157_0 \pm 0.006_2$ and $b = (1.81_1 \pm 0.19_0) \times 10^{-4}$ s^{-1} (the reported uncertainties represent 2σ from the statistical analysis).

loss of SF_6 in the chamber can be reasonably well approximated by the expression:

$$\ln\{[SF_6]_0/[SF_6]_t\} = \int_0^t k_{leak}(t)\,dt = a(1 - \exp(-bt)) \quad (5)$$

in which $[SF_6]_0$ and $[SF_6]_t$ are the initial SF_6 concentration and that after a time t, respectively, and a and b are constants. The leak rate coefficient is then given by $k_{leak}(t) = ab\exp(-bt)$. The reason for this curvature is not known: it was apparently not caused by inadequate mixing (the fans were operating properly), but more likely caused by improper regulation of the pressure in the beginning of the experiment (too high pressure inside the chamber compared to the pressure outside). In any case, as long as the leakage rate we extract is close to the "true" leakage rate, our experimental data will not be seriously affected. Fitting eq 5 to the data points in Figure 8 gives the following values for the regression coefficients (the reported uncertainty is 2σ from the statistical analysis): $a = 0.157_0 \pm 0.006_2$; $b = (1.81_1 \pm 0.19_0) \times 10^{-4}$ s^{-1}.

In Figure 9 the time variation of J_{max} during the day of the experiment is plotted. As can be seen, J_{max} is fairly constant between 11:00 and 14:30 GMT, but changes significantly with time outside this interval. We have used two different approaches to extract the effective quantum yield of photolysis, eq 3. In the first approach Φ_{eff} have been fitted directly, using FACSIMILE,[39] to the experimental concentrations of CHF_2CHO and DNBE according to the differential equations describing the reaction scheme given in Table 2. This allows us to use the whole time period of the experiment. The FACSIMILE code is given in Table S1. Figure 9 shows the results from this approach and an effective quantum yield of photolysis of 0.31 $\pm$ 0.03 was extracted. The reported uncertainty reflects 2σ from the statistical analysis and includes the uncertainty in the OH rate coefficient of CHF_2CHO and the uncertainty in the leakage rate. Since the OH reaction rate of CHF_2CHO is relatively slow compared to the photolysis rate, the effective quantum yield of photolysis is not very sensitive to the OH concentration used in the model. Using a constant OH concentration of 1×10^6 radicals cm^{-3} does not change the derived Φ_{eff} significantly (but the agreement with the di-*n*-butyl ether concentration profile is of course sensitive to the OH concentration).

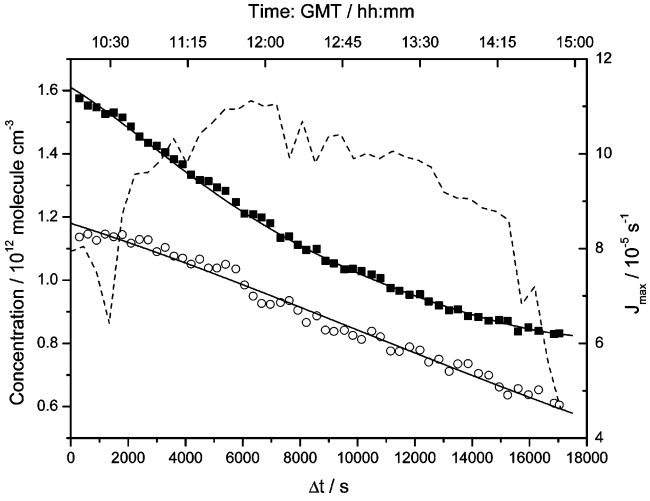

Figure 9. Observed total loss of (■) CHF_2CHO and (○) $(C_4H_9)_2O$ in the EUPHORE simulation chamber corrected for variations in pressure and temperature. The concentrations are given in units of molecule cm^{-3}.

In the second approach we assumed J_{obs} to be constant in which case the differential equations for the reaction scheme in Table 1 have an analytical solution:

$$\ln\left\{\frac{[CHF_2CHO]_0}{[CHF_2CHOI]_t}\right\} - \frac{k_{ald}}{k_{DNBE}}\ln\left\{\frac{[(C_4H_9)_2O]_0}{[(C_4H_9)2O]_t}\right\} - \left(1 - \frac{k_{ald}}{k_{DNBE}}\right)a[1 - \exp(-bt)] = J_{obs}t \quad (6)$$

Here $[...]_0$ and $[...]_t$ are the concentrations of CHF_2CHO and $(C_4H_9)_2O$ at the start and after a time t, respectively, $k_{ald} = k(OH+CHF_2CHO) = 1.8 \times 10^{-12}$ cm^3 molecule^{-1} s^{-1} (this work), and $k_{DNBE} = k(OH+(C_4H_9)_2O) = 2.89 \times 10^{-11}$ cm^3 molecule^{-1} s^{-1}.[46] Figure 10 shows the total loss of CHF_2CHO in the chamber and the loss of CHF_2CHO after corrections for variations in pressure and temperature and for reaction with OH radicals and leakage according to eq 6. From least-squares analysis of the data points from 11:00 to 14:30 GMT an observed photolysis rate of $(2.91 \pm 0.09) \times 10^{-5}$ s^{-1} (2σ; precision only) was extracted. The time averaged maximum photolysis rate, J_{max} (see eq 4), during the experiment was calculated to be 9.8×10^{-5} s^{-1}, which gives $\Phi_{eff} = 0.30 \pm 0.03$ (uncertainty in OH rate coefficient and leakage rate coefficient included also). Thus, the two very different approaches to derive the effective quantum yield to photolysis result in essentially the same value. It is not obvious that the leakage rate of CHF_2CHO is exactly the same as that of SF_6. It is therefore likely that the uncertainty in the experiment is larger than that given above. We therefore prefer to report $\Phi_{eff} = 0.30 \pm 0.05$ for the tropospheric photolysis of 2,2-difluoroacetaldehyde.

An effective quantum yield of 0.30 $\pm$ 0.05 is remarkably different from what has been observed for CH_3CHO and CF_3CHO under similar conditions in the EUPHORE simulation chamber. For CH_3CHO a quantum yield of 0.06 $\pm$ 0.1 has been reported,[59] while an upper limit of 0.01 has been reported for CF_3CHO.[36] This instantly brings forward the question: why are the quantum yields to photolysis of these related molecules so different?

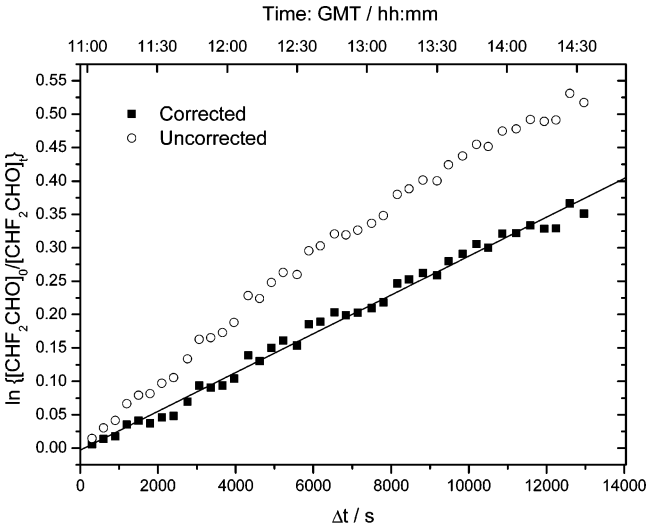

Figure 10. (○) Total loss of CHF_2CHO in the EUPHORE simulation chamber, Valencia, Spain. The data points are not corrected for variations in pressure and temperature. (■) Observed loss of CHF_2CHO after correcting for variations in pressure and temperature and for loss due to OH reactions and leakage according to eq 6. Least-squares fit gave $J_{obs} = (2.91 \pm 0.09) \times 10^{-5}$ s^{-1} (2σ; precision only); y-intercept: 0.003 ± 0.006. The time averaged J_{max}, eq 4, during this time period was 9.8×10^{-5} s^{-1}.

To unravel the mechanisms behind these observations, we have performed a series of quantum chemical calculations on the photodissociation pathways of CH_3CHO, CH_2FCHO, CHF_2CHO, and CF_3CHO. The photolytical processes under study can be described as

$$\mathrm{RCHO} + h\nu \rightarrow \mathrm{RH} + \mathrm{CO}\ \text{(molecular channel)} \quad (7)$$

$$\rightarrow \mathrm{R} + \mathrm{HCO}\ \text{(radical channel)} \quad (8)$$

$$\rightarrow \mathrm{RCO} + \mathrm{H}\ \text{(radical channel)} \quad (9)$$

where R symbolizes a CH_3, CH_2F, CHF_2, or CF_3 group. The molecular channel is thought to take place on the singlet ground-state potential energy surface (S_0), while the radical channels occur on the lowest triplet surface (T_1). Although the radical channels in principle also can take place on the S_1 surface as observed for acetone,[60] it is unlikely that this will occur for $\lambda > 310$ nm (the actinic flux is very low below 310 nm in the troposphere). Consequently, we have ignored this possibility here.

We have tested the MP2 and B3LYP models to find the best computational approach, using acetaldehyde for benchmarking (a multi-configurational approach would be too time-consuming). Additional CASSCF calculations have been performed on acetaldehyde. Figures S6a−e (Supporting Information) display the stationary points involved in the photolysis of acetaldehyde, for the CAS(8,7), CAS(12,12), MP2, and B3LYP models in the aug-cc-pVDZ basis. We here discuss the results for the aug-cc-pVDZ basis, the only basis used for all models. All geometrical data are given in Tables S2−6 (Supporting Information).

For the S_0 surface, the agreement between the different models is good, both for the minimum, Figure S6a (Supporting Information), and for the TS1 transition state of the molecular channel, Figure S6c (Supporting Information). The CAS(8,7) minimum structure agrees well with the MP2 and B3LYP structures, bearing in mind that no methyl C−H orbitals were active. The CAS(12,12) model overestimates bond lengths by 0.5 to 2 pm, the active space being too small for dynamical correlation.

TABLE 3: Comparison of Relative Energies for the Different Barriers toward Photodissociation of CH_3CHO Calculated at Several Levels of Theory (zero-point vibrational energies are included)[a]

	ΔE/kJ mol^{-1}		
	TS1-S_0	TS2-T_1	TS3-T_1
this work			
MP2(FC)/aug-cc-pVDZ	347.6	53.2	68.7
MP2(FC)/aug-cc-pVTZ	346.9	51.4	69.5
B3LYP/aug-cc-pVDZ	338.4	57.7	84.4
B3LYP/aug-cc-pVTZ	336.6	52.8	84.3
B3LYP/aug-cc-pVQZ	337.1	53.7	84.3
CAS(8,7)/aug-cc-pVDZ	376.2	49.8	60.7
CAS(12,12)/aug-cc-pVDZ	313.7	19.2	40.0
literature data			
Yadav and Goddard[71,b]	353.1	51.5	64.9
Kurosaki and Yokoyama[62,c]	352.3, 341.4, 348.1		
Setokuchi et al.[61,d]		51.8	83.9
King et al.[72,e]		44.6	
Kurosaki and Yokoyama[73,f]		59.8, 61.9	

[a] The geometries of the different stationary points are displayed in Figure S6a−e and Tables S2−6 [b] HF/3-21G + thermal + HF/6-31G* + CISD/3-21G + SCC/3-21G. [c] RMP2(full)/cc-pVDZ//RMP2(full)/cc-pVDZ; RMP4(SDTQ,full)/cc-pVTZ//RMP2(full)/cc-pVDZ; RQ-CISD(T,full)/cc-pVTZ//RMP2(full)/cc-pVDZ. [d] MRMP/TZV(2df,2p)//CAS(10,10)/cc-pVDZ. [e] Valence focal-point analysis. [f] B3LYP/cc-pVDZ; MP2(full)/cc-pVDZ.

On the T_1 surface, the MP2 and B3LYP differences are larger. The MP2 C−C bond of the TS3 transition state (Figure S6e, Supporting Information), in particular, is 3 to 4 pm longer than the B3LYP and CAS bonds. As usual, the MP2 model suffers more from spin contamination than does the B3LYP model. At the minimum, $\langle S^2 \rangle$ is 2.017 at the MP2 level of theory but only 2.006 at the B3LYP level. The largest contamination occurs for TS3, where $\langle S^2 \rangle$ is 2.091 at the MP2 level and 2.014 at the B3LYP level.

The computed dissociation barriers are given in Table 3, along with relevant literature values. Only calculated barrier heights have been included from the literature since an experimentally determined barrier does not necessarily reflect the energy of the transition state—it may also reflect the energy of the intersection between the surfaces involved. Setokuchi et al.[61] have described the bond breaking process with a multi-configurational wave function (CAS(10,10)/cc-pVDZ) and dynamical correlation by multireference Møller−Plesset (MRMP) theory, providing the highest computational level among the cited studies. Whereas the B3LYP calculations are in good agreement with their study, the MP2 model gives a too low TS3 transition state. For ΔE(TS1-S_0), the B3LYP model predicts lower barriers than reported by Kurosaki and Yokoyama,[62] while the MP2 model is in better agreement. The poor CAS barrier heights arise from the absence of dynamical correlation.

In short, the MP2 and B3LYP models describe the S_0 bond-breaking process well compared with the CAS and literature values, although the B3LYP model predicts a too low barrier for the dissociation into CH_4 and CO. However, the B3LYP model is better at describing the T_1 bond breaking than is the MP2 model. We conclude that the B3LYP model is the best one for describing these bond-breaking processes, with no obvious errors.

The stationary points of CH_2FCHO, CHF_2CHO, and CF_3CHO are displayed in Figures S7a−f, S8a−e, and S9a−e (Supporting Information), respectively. Energy level diagrams for the dissociation routes involved in the photolysis of CH_3CHO, CH_2FCHO, CHF_2CHO, and CF_3CHO calculated at the B3LYP/aug-cc-pVQZ level of theory are shown in Figure 11a−

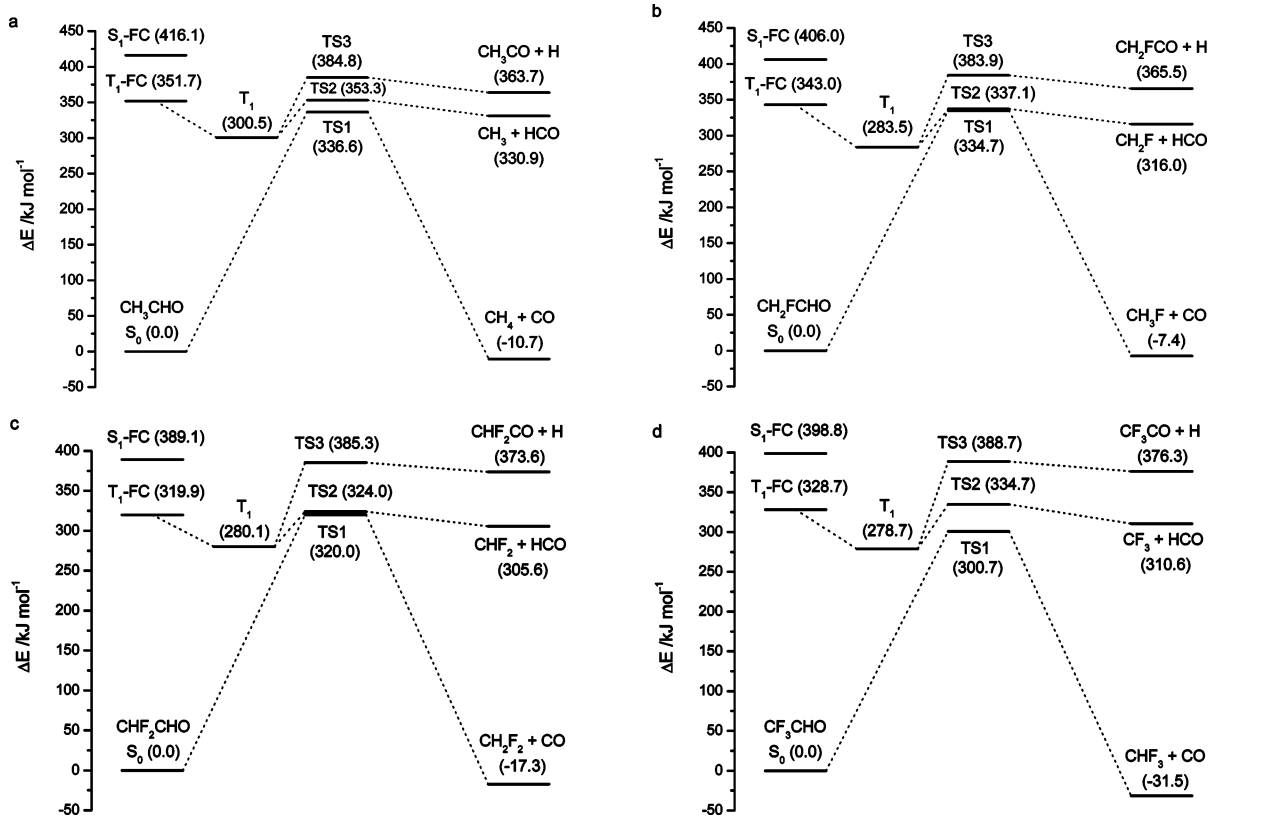

Figure 11. Energy level diagrams for the different dissociation routes involved in the photolysis of (a) CH_3CHO, (b) CH_2FCHO, (c) CHF_2CHO, and (d) CF_3CHO calculated at the B3LYP/aug-cc-pVQZ level of theory (zero-point vibrational energies included). The Franck−Condon (FC) energies have been calculated by using TD-B3LYP/aug-cc-pVQZ. The geometries of the stationary points involved are given in Figures S6a−e (CH_3CHO), S7a−f (CH_2FCHO), S8a−e (CHF_2CHO), and S9a−e (CF_3CHO) in the Supporting Information.

d, with the acetaldehyde diagram included for completeness. The Franck−Condon (FC) regions have been explored by using TD-B3LYP/aug-cc-pVQZ. As seen from Figure 11a−d, the calculations correctly reproduce the observed red shifts of the UV spectra of CHF_2CHO and CF_3CHO compared to those of CH_3CHO.

Starting with the dissociation channel in eq 7, we note that the TS1 barrier decreases in the series CH_3CHO, CH_2FCHO, CHF_2CHO, and CF_3CHO, the calculated CF_3CHO barrier being 36 kJ mol^{-1} lower than the CH_3CHO barrier. For the radical channel in eq 8, the barrier height (TS2) relative to the S_0 minimum decreases upon fluorination except for CHF_2CHO, which has the lowest barrier. Relative to the T_1 minimum, the TS2 barrier height is 53 kJ mol^{-1} for CH_3CHO, 54 kJ mol^{-1} for CH_2FCHO, and 56 kJ mol^{-1} for CF_3CHO, but only 44 kJ mol^{-1} for CHF_2CHO. The channel in eq 9 is the least favorable path, with the largest barrier heights (TS3). We therefore do not discuss this path any further.

A first interpretation of these results would be to suggest that CF_3CHO is easiest to photolyze, having the lowest dissociation barrier (TS1) and being electronically allowed. However, this and previous experimental studies on acetaldehyde[59] and 2,2,2-difluoroacetaldehyde[36] have showed that the photolysis of CF_3CHO is much slower than the photolysis of CH_3CHO and CHF_2CHO in the EUPHORE chamber under similar sunlight conditions. We must therefore look for a different interpretation.

Since these photodissociations are predissociations, crossings between the electronic surfaces must also be considered. If the photolytical reaction in eq 7 is to occur under tropospheric conditions, a conical intersection (CI)[63] between the S_1 and S_0 surfaces must be accessible. Similarly, an intersystem crossing (ISC) between the S_1 and T_1 surfaces must be accessible for the routes in eqs 8 and 9. Since no calculations of such intersections have been reported in the literature, we attempted to characterize the CI/ISC for acetaldehyde (CAS calculations using Gaussian 03[64]). The calculations are complicated since the intersections do not lie on the minimum energy path. Only one S_1/S_0 CI of too high energy was located. Moreover, we were unable to find any S_1/T_1 ISC, only regions where the surfaces are close. Still, experimental studies suggest that the dissociation of acetaldehyde into CH_3 and HCO is the dominant reaction route at wavelengths relevant to the troposphere (see e.g. refs 65−67). Since the energy of TS1 is lower than the energy of TS2 relative to the S_0 minimum for acetaldehyde, the conical intersection S_1/S_0 should have a higher energy than the intersystem crossing S_1/T_1.

Concerning CF_3CHO, it seems that no intersection is available at wavelengths longer than 290 nm (fluorescence has been observed down to 270 nm in laser-induced fluorescence experiments[68]). The photodissociation of CF_3CHO may instead occur on the S_1 surface.

For CHF_2CHO, at least one energetically available intersection exists. In the photolysis study carried out in the Oslo reaction chamber, CF_2O was the major fluorinated product (no other could be detected, see Figure S1, Supporting Information), suggesting that dissociation of CHF_2CHO into CHF_2 and HCO is the dominant reaction route. To strengthen this case, we note from Figure 11a−d that the energy gap between TS1 (being a singlet state) and TS2 (being a triplet state) is largest for CF_3CHO and smallest for CH_2FCHO and CHF_2CHO. Since the transition state structures of CHF_2CHO and CF_3CHO are similar, this suggests that the singlet and triplet surfaces are less repulsive for CHF_2CHO than for CF_3CHO, which again increases the probability of finding an intersystem crossing.

To conclude, our quantum chemical calculations have shown that the observed photolysis rates of CH_3CHO, CHF_2CHO, and CF_3CHO cannot solely be explained by differences in the barrier heights TS1 and TS2 toward dissociation. Rather, the experimental observations should be explained in terms of low-lying intersections between the electronic states involved in the photodissociation processes. Future computational studies on these photolytic systems should focus on such intersections.

4. Atmospheric Implications

The atmospheric lifetime of 2,2-difluoroacetaldehyde due to removal by reaction with OH radicals and photolysis may be estimated from the data obtained in this work. The atmospheric lifetime is given by $\tau^{-1} = \tau_{OH}{}^{-1} + \tau_{photol}{}^{-1}$. Using the OH reaction rate coefficient determined in this work (1.8×10^{-12} cm^3 $molecule^{-1}$ s^{-1}) and a global average OH concentration of 9.4×10^5 radicals cm^{-3},[69] we find that $\tau_{OH} \sim 7$ days. The photolytic lifetime can be estimated by using the time-averaged value of $J_{obs} = 2.82 \times 10^{-5}$ s^{-1}. Correcting for the transmission of the FEP foil of the EUPHORE chamber (75%) gives a photolytic lifetime of 8 h under conditions with $\langle J(NO_2)\rangle = 8.6 \times 10^{-3}$ s^{-1}. Fluorinated aldehydes are fairly water soluble and undergo hydrolysis and oxidation forming the corresponding carboxylic acids. Based on the work of de Bruyn et al.,[70] it is estimated that τ_{uptake} of CHF_2CHO is of the order of 5−30 days. Hence, the atmospheric lifetime of 2,2-difluoroacetaldehyde is determined by photolysis, which is somewhat surprising. Given the experimental uncertainties a conservative estimate of the atmospheric lifetime of 2,2-difluoroacetaldehyde is therefore around 1 day.

The available data suggest that CF_2O will be the major product in the gas-phase oxidation of CHF_2CHO although CH_2F_2 could be formed in one of the photolytic reaction routes. CH_2F_2 will, however, be oxidized to CF_2O in the atmosphere. CF_2O is rapidly (∼3 days) incorporated into raindrops/aerosols and hydrolyzed to HF and CO_2.[70] The environmental burden of CHF_2CHO is therefore negligible.

Acknowledgment. This work is part of the project "Impact of Fluorinated Alcohols and Ethers on the Environment", and has received support from the Commission of the European Communities under the Energy, Environment and Sustainable Development Programme through contract EVK2-CT-1999-00009. The High Performance Computing Centre at the University of Oslo is acknowledged for grants of computing time. We thank Klaus Wirtz and his team for all their help during the stay at EUPHORE. Prof. Michael A. Robb is acknowledged for helpful discussions concerning conical intersections.

Supporting Information Available: Absolute infrared and ultraviolet−visible absorption cross sections (base e) of CHF_2CHO are given in JCAMP-DX format; FACSIMILE code for fitting the effective quantum yield of photolysis to experimental data as observed in EUPHORE simulation chamber (Table S1); calculated geometrical parameters for the singlet ground-state equilibrium of CH_3CHO (Table S2), the triplet ground-state equilibrium of CH_3CHO (Table S3), the transition state toward $CH_3CHO \rightarrow CH_4 + CO$ (Table S4), the transition state toward $CH_3CHO \rightarrow CH_3 + HCO$ (Table S5), and the transition state toward $CH_3CHO \rightarrow CH_3CO + H$ (Table S6); difference FTIR spectrum after 45 min of photolysis of CHF_2CHO at λ_{max} ∼310 nm (Figure S1); decay of CHF_2CHO due to photolysis at λ_{max} ∼310 nm (Figure S2); FTIR spectra of the reaction mixture $CHF_2CHO/C_2H_6/Cl_2$ (Figure S3); FTIR spectra of the reaction mixture $CHF_2CHO/(E)\text{-}C_2H_2Cl_2/NO_3$ (Figure S4); computed structures of stationary points on the potential energy surface of the $CHF_2CHO + OH$ reaction system (Figure S5a−h); Computed geometrical parameters of stationary points involved in the photolysis of CH_3CHO (Figure S6a−e), CH_2FCHO (Figure S7a−f), CHF_2CHO (Figure S8a−e), and CF_3CHO (Figure S9a−e). This material is available free of charge via the Internet at http://pubs.acs.org.

References and Notes

(1) Papadimitriou, V. C.; Prosmitis, A. V.; Lazarou, Y. G.; Papagiannakopoulos, P. *J. Phys. Chem. A* **2003**, *107*, 3733.
(2) Sellevåg, S. R.; Nielsen, C. J.; Søvde, O. A.; Myhre, G.; Sundet, J. K.; Stordal, F.; Isaksen, I. S. A. *Atmos. Environ.* **2004**, *38*, 6725.
(3) Scollard, D. J.; Treacy, J. J.; Sidebottom, H. W.; Balestra-Garcia, C.; Laverdet, G.; LeBras, G.; MacLeod, H.; Teton, S. *J. Phys. Chem.* **1993**, *97*, 4683.
(4) Oyaro, N.; Sellevåg, S. R.; Nielsen, C. J. *Environ. Sci. Technol.* **2004**, *38*, 5567.
(5) Oyaro, N.; Sellevåg, S. R.; Nielsen, C. J. *J. Phys. Chem. A* **2005**, *109*, 337.
(6) McBee, E. T.; Pierce, O. R.; Hsu, C. G. *Proc. Indiana Acad. Sci.* **1955**, *64*, 108.
(7) Yamada, B.; Campbell, R. W.; Vogl, O. *Polym. J.* (*Tokyo*) **1977**, *9*, 23.
(8) Kaneko, S.; Yamazaki, T.; Kitazume, T. *J. Org. Chem.* **1993**, *58*, 2302.
(9) Aker, P. M.; Sloan, J. J. *J. Chem. Phys.* **1986**, *85*, 1412.
(10) Huang, Y.; Gu, Y.; Liu, C.; Yang, X.; Tao, Y. *Chem. Phys. Lett.* **1986**, *127*, 432.
(11) Streit, G. E.; Whitten, G. Z.; Johnston, H. S. *Geophys. Res. Lett.* **1976**, *3*, 521.
(12) D′Ottone, L.; Bauer, D.; Campuzano-Jost, P.; Fardy, M.; Hynes, A. J. *Phys. Chem. Chem. Phys.* **2004**, *6*, 4276.
(13) Becker, K. H. The European Photoreactor EUPHORE. Design and Technical Development of the European Photoreactor and First Experimental Results; Final Report of the EC-Project Contract EV5V-CT92-0059, Wuppertal, 1996.
(14) Klotz, B.; Sorensen, S.; Barnes, I.; Becker, K. H.; Etzkorn, T.; Volkamer, R.; Platt, U.; Wirtz, K.; Martin-Reviejo, M. *J. Phys. Chem. A* **1998**, *102*, 10289.
(15) Magneron, I.; Thevenet, R.; Mellouki, A.; Le Bras, G.; Moortgat, G. K.; Wirtz, K. *J. Phys. Chem. A* **2002**, *106*, 2526.
(16) Volkamer, R.; Platt, U.; Wirtz, K. *J. Phys. Chem. A* **2001**, *105*, 7865.
(17) Wenger, J. C.; Le Calve, S.; Sidebottom, H. W.; Wirtz, K.; Reviejo, M. M.; Franklin, J. A. *Environ. Sci. Technol.* **2004**, *38*, 831.
(18) Møller, C.; Plesset, M. S. *Phys. Rev.* **1934**, *46*, 618.
(19) Becke, A. D. *J. Chem. Phys.* **1993**, *98*, 5648.
(20) Lee, C.; Yang, W.; Parr, R. G. *Phys. Rev. B* **1988**, *37*, 785.
(21) Raghavachari, K.; Trucks, G. W.; Pople, J. A.; Head-Gordon, M. *Chem. Phys. Lett.* **1989**, *157*, 479.
(22) Frisch, M. J.; Trucks, G. W.; Schlegel, H. B.; Scuseria, G. E.; Robb, M. A.; Cheeseman, J. R.; Zakrzewski, V. G.; Montgomery, J. A., Jr.; Stratmann, R. E.; Burant, J. C.; Dapprich, S.; Millam, J. M.; Daniels, A. D.; Kudin, K. N.; Strain, M. C.; Farkas, O.; Tomasi, J.; Barone, V.; Cossi, M.; Cammi, R.; Mennucci, B.; Pomelli, C.; Adamo, C.; Clifford, S.; Ochterski, J.; Petersson, G. A.; Ayala, P. Y.; Cui, Q.; Morokuma, K.; Salvador, P.; Dannenberg, J. J.; Malick, D. K.; Rabuck, A. D.; Raghavachari, K.; Foresman, J. B.; Cioslowski, J.; Ortiz, J. V.; Baboul, A. G.; Stefanov, B. B.; Liu, G.; Liashenko, A.; Piskorz, P.; Komaromi, I.; Gomperts, R.; Martin, R. L.; Fox, D. J.; Keith, T.; Al-Laham, M. A.; Peng, C. Y.; Nanayakkara, A.; Challacombe, M.; Gill, P. M. W.; Johnson, B.; Chen, W.; Wong, M. W.; Andres, J. L.; Gonzalez, C.; Head-Gordon, M.; Replogle, E. S.; Pople, J. A. *Gaussian 98*, Revision A.11; Gaussian, Inc.: Pittsburgh, PA, 2001.
(23) Dunning, T. H., Jr. *J. Chem. Phys.* **1989**, *90*, 1007.
(24) Kendall, R. A.; Dunning, T. H., Jr.; Harrison, R. J. *J. Chem. Phys.* **1992**, *96*, 6796.
(25) Gross, E. K. U.; Kohn, W. *Adv. Quantum Chem.* **1990**, *21*, 255.
(26) Stratmann, R. E.; Scuseria, G. E.; Frisch, M. J. *J. Chem. Phys.* **1998**, *109*, 8218.
(27) Jensen, H. J. A.; Aagren, H. *Chem. Phys. Lett.* **1984**, *110*, 140.
(28) Jensen, H. J. A.; Aagren, H. *Chem. Phys.* **1986**, *104*, 229.
(29) Helgaker, T.; Aa. Jensen, H. J.; Joergensen, P.; Olsen, J.; Ruud, K.; Aagren, H.; Auer, A. A.; Bak, K. L.; Bakken, V.; Christiansen, O.; Coriani, S.; Dahle, P.; Dalskov, E. K.; Enevoldsen, T.; Fernandez, B.; Haettig, C.; Hald, K.; Halkier, A.; Heiberg, H.; Hettema, H.; Jonsson, D.; Kirpekar, S.; Kobayashi, R.; Koch, H.; Mikkelsen, K. V.; Norman, P.; Packer, M. J.; Pedersen, T. B.; Ruden, T. A.; Sanchez, A.; Saue, T.; Sauer,

S. P. A.; Schimmelpfennig, B.; Sylvester-Hvid, K. O.; Taylor, P. R.; Vahtras, O. *Dalton*, a molecular electronic structure program, Release 1.2, 2001.

(30) Aa. Jensen, H. J.; Jørgensen, P.; Ågren, H.; Olsen, J. *J. Chem. Phys.* **1988**, *88*, 3834.

(31) Ballard, J.; Knight, R. J.; Newnham, D. A.; Vander Auwera, J.; Herman, M.; Di Lonardo, G.; Masciarelli, G.; Nicolaisen, F. M.; Beukes, J. A.; Christensen, L. K.; McPheat, R.; Duxbury, G.; Freckleton, R.; Shine, K. P. *J. Quant. Spectrosc. Radiat. Transfer* **2000**, *66*, 109.

(32) Martinez, R. D.; Buitrago, A. A.; Howell, N. W.; Hearn, C. H.; Joens, J. A. *Atmos. Environ., Part A* **1992**, *26A*, 785.

(33) Francisco, J. S.; Williams, I. H. *Mol. Phys.* **1992**, *76*, 1433.

(34) Libuda, H.-G. Spektroskopische und kinetische untersuchungen an halogenierten carbonylverbindungen von atmosphärischem interesse. Ph.D. Thesis, Bergischen Universität-Gesamthochschule, 1992.

(35) Meller, R.; Boglu, D.; Moortgat, G. K. Absorption cross-section and photolysis studies of halogenated carbonyl compounds. Photooxidation of CF3-containing CFC-substitutes; STEP-HALOCSIDE/AFEAS Workshop; March 23−25, Dublin, 1993; p 130.

(36) Sellevåg, S. R.; Kelly, T.; Sidebottom, H.; Nielsen, C. J. *Phys. Chem. Chem. Phys.* **2004**, *6*, 1243.

(37) Hashikawa, Y.; Kawasaki, M.; Waterland, R. L.; Sulbaek Andersen, M. P.; Nielsen, O. J.; Hurley, M. D.; Ball, J. C.; Wallington, T. J. Gas-phase UV and IR absorption spectra of $C_xF_{2x+1}CHO$ ($x = 1-4$); The Fifth Informal Conference on Reaction Kinetics and Atmospheric Chemistry; June 11−13, LO-skolen Conference Center; Helsingør; Rosenørn, T., Langer, S., Johnson, M. S., Eds.; University of Copenhagen, Denmark, 2004; pp Poster A4.

(38) York, D. *Can. J. Phys.* **1966**, *44*, 1079.

(39) FACSIMILE for Windows, Version 4.0.31; MCPA Software Ltd.

(40) Sander, S. P.; Friedl, R. R.; Golden, D. M.; Kurylo, M. J.; Huie, R. E.; Orkin, V. L.; Moortgat, G. K.; Ravishankara, A. R.; Kolb, C. E.; Molina, M. J.; Finlayson-Pitts, B. J. Chemical Kinetics and Photochemical Data for Use in Atmospheric Studies. Evaluation Number 14; JPL Publication 02-25; National Aeronautics and Space Administration, Jet Propulsion Laboratory, California Institute of Technology, Pasadena, CA, 2003.

(41) Atkinson, R.; Baulch, D. L.; Cox, R. A.; Crowley, J. N.; Hampson, R. F., Jr.; Hynes, R. G.; Jenkin, M. E.; Kerr, J. A.; Rossi, M. J.; Troe, J. Summary of evaluated kinetic and photochemical data for atmospheric chemistry; IUPAC Subcommittee on Gas Kinetic Data Evaluation for Atmospheric Chemistry, Web Version July 2004; http://www.iupac-kinetic.ch.cam.ac.uk/.

(42) Atkinson, R. *J. Phys. Chem. Ref. Data, Monogr.* **1989**, *1*, 1.

(43) Atkinson, R. *J. Phys. Chem. Ref. Data, Monogr.* **1994**, *2*, 1.

(44) Semadeni, M.; Stocker, D. W.; Kerr, J. A. *Int. J. Chem. Kinet.* **1995**, *27*, 287.

(45) Anderson, P. N.; Hites, R. A. *Environ. Sci. Technol.* **1996**, *30*, 301.

(46) Kramp, F.; Paulson, S. E. *J. Phys. Chem. A* **1998**, *102*, 2685.

(47) Bohn, B. *J. Phys. Chem. A* **2001**, *105*, 6092.

(48) Wallington, T. J.; Andino, J. M.; Ball, J. C.; Japar, S. M. *J. Atmos. Chem.* **1990**, *10*, 301.

(49) Atkinson, R.; Aschmann, S. M.; Goodman, M. A. *Int. J. Chem. Kinet.* **1987**, *19*, 299.

(50) Noremsaune, I. M.; Langer, S.; Ljungstroem, E.; Nielsen, C. J. *J. Chem. Soc., Faraday Trans.* **1997**, *93*, 525.

(51) D'Anna, B.; Andresen, O.; Gefen, Z.; Nielsen, C. J. *Phys. Chem. Chem. Phys.* **2001**, *3*, 3057.

(52) D'Anna, B.; Bakken, V.; Beukes, J. A.; Nielsen, C. J.; Brudnik, K.; Jodkowski, J. T. *Phys. Chem. Chem. Phys.* **2003**, *5*, 1790.

(53) Löwdin, P.-O. *Rev. Mod. Phys.* **1963**, *35*, 496.

(54) Eisfeld, W.; Morokuma, K. *J. Chem. Phys.* **2000**, *113*, 5587.

(55) Aloisio, S.; Francisco, J. S. *J. Phys. Chem. A* **2000**, *104*, 3211.

(56) Alvarez-Idaboy, J. R.; Mora-Diez, N.; Boyd, R. J.; Vivier-Bunge, A. *J. Am. Chem. Soc.* **2001**, *123*, 2018.

(57) Mora-Diez, N.; Alvarez-Idaboy, J. R.; Boyd, R. J. *J. Phys. Chem. A* **2001**, *105*, 9034.

(58) Smith, I. W. M.; Ravishankara, A. R. *J. Phys. Chem. A* **2002**, *106*, 4798.

(59) Moortgat, G. K. Evaluation of Radical Sources in Atmospheric Chemistry through Chamber and Laboratory Studies: RADICAL; Final report on EU project ENV4-CT97-0419; Max-Planck-Institut für Chemie, Atmospheric Chemistry Divition, Mainz, Germany, 2000.

(60) Diau, E. W. G.; Kotting, C.; Zewail, A. H. *ChemPhysChem* **2001**, *2*, 273.

(61) Setokuchi, O.; Matuzawa, S.; Shimizu, Y. *Chem. Phys. Lett.* **1998**, *284*, 19.

(62) Kurosaki, Y.; Yokoyama, K. *J. Phys. Chem. A* **2002**, *106*, 11415.

(63) Bernardi, F.; Olivucci, M.; Robb, M. A. *Chem. Soc. Rev.* **1996**, *25*, 321.

(64) Frisch, M. J.; Trucks, G. W.; Schlegel, H. B.; Scuseria, G. E.; Robb, M. A.; Cheeseman, J. R.; Montgomery, J. A., Jr.; Vreven, T.; Kudin, K. N.; Burant, J. C.; Millam, J. M.; Iyengar, S. S.; Tomasi, J.; Barone, V.; Mennucci, B.; Cossi, M.; Scalmani, G.; Rega, N.; Petersson, G. A.; Nakatsuji, H.; Hada, M.; Ehara, M.; Toyota, K.; Fukuda, R.; Hasegawa, J.; Ishida, M.; Nakajima, T.; Honda, Y.; Kitao, O.; Nakai, H.; Klene, M.; Li, X.; Knox, J. E.; Hratchian, H. P.; Cross, J. B.; Adamo, C.; Jaramillo, J.; Gomperts, R.; Stratmann, R. E.; Yazyev, O.; Austin, A. J.; Cammi, R.; Pomelli, C.; Ochterski, J. W.; Ayala, P. Y.; Morokuma, K.; Voth, G. A.; Salvador, P.; Dannenberg, J. J.; Zakrzewski, V. G.; Dapprich, S.; Daniels, A. D.; Strain, M. C.; Farkas, O.; Malick, D. K.; Rabuck, A. D.; Raghavachari, K.; Foresman, J. B.; Ortiz, J. V.; Cui, Q.; Baboul, A. G.; Clifford, S.; Cioslowski, J.; Stefanov, B. B.; Liu, G.; Liashenko, A.; Piskorz, P.; Komaromi, I.; Martin, R. L.; Fox, D. J.; Keith, T.; Al-Laham, M. A.; Peng, C. Y.; Nanayakkara, A.; Challacombe, M.; Gill, P. M. W.; Johnson, B.; Chen, W.; Wong, M. W.; Gonzalez, C.; Pople, J. A. *Gaussian 03*, Revision B.03; Gaussian, Inc.: Pittsburgh, PA, 2003.

(65) Parmenter, C. S.; Noyes, W. A., Jr. *J. Am. Chem. Soc.* **1963**, *85*, 416.

(66) Horowitz, A.; Kershner, C. J.; Calvert, J. G. *J. Phys. Chem.* **1982**, *86*, 3094.

(67) Horowitz, A.; Calvert, J. G. *J. Phys. Chem.* **1982**, *86*, 3105.

(68) Temps, F. Private communication.

(69) Prinn, R. G.; Huang, J.; Weiss, R. F.; Cunnold, D. M.; Fraser, P. J.; Simmonds, P. G.; McCulloch, A.; Harth, C.; Salameh, P.; O'Doherty, S.; Wang, R. H. J.; Porter, L.; Miller, B. R. *Science* **2001**, *292*, 1882.

(70) de Bruyn, W. J.; Shorter, J. A.; Davidovits, P.; Worsnop, D. R.; Zahniser, M. S.; Kolb, C. E. *Environ. Sci. Technol.* **1995**, *29*, 1179.

(71) Yadav, J. S.; Goddard, J. D. *J. Chem. Phys.* **1986**, *84*, 2682.

(72) King, R. A.; Allen, W. D.; Schaefer, H. F., III *J. Chem. Phys.* **2000**, *112*, 5585.

(73) Kurosaki, Y.; Yokoyama, K. *Chem. Phys. Lett.* **2003**, *371*, 568.